Environmental Science & Technology

pubs.acs.org/est

Article

Ammonia Dry Deposition in an Alpine Ecosystem Traced to Agricultural Emission Hotpots

Da Pan, Katherine B. Benedict, Levi M. Golston, Rui Wang, Jeffrey L. Collett, Jr, Lei Tao, Kang Sun, Xuehui Guo, Jay Ham, Anthony J. Prenni, Bret A. Schichtel, Tomas Mikoviny, Markus Müller, Armin Wisthaler, and Mark A. Zondlo*

Cite This: *Environ. Sci. Technol.* 2021, 55, 7776−7785

Read Online

ACCESS | Metrics & More | Article Recommendations | Supporting Information

ABSTRACT: Elevated reactive nitrogen (N_r) deposition is a concern for alpine ecosystems, and dry NH_3 deposition is a key contributor. Understanding how emission hotspots impact downwind ecosystems through dry NH_3 deposition provides opportunities for effective mitigation. However, direct NH_3 flux measurements with sufficient temporal resolution to quantify such events are rare. Here, we measured NH_3 fluxes at Rocky Mountain National Park (RMNP) during two summers and analyzed transport events from upwind agricultural and urban sources in northeastern Colorado. We deployed open-path NH_3 sensors on a mobile laboratory and an eddy covariance tower to measure NH_3 concentrations and fluxes. Our spatial sampling illustrated an upslope event that transported NH_3 emissions from the hotspot to RMNP. Observed NH_3 deposition was significantly higher when backtrajectories passed through only the agricultural region (7.9 ng m^{-2} s^{-1}) versus only the urban area (1.0 ng m^{-2} s^{-1}) and both urban and agricultural areas (2.7 ng m^{-2} s^{-1}). Cumulative NH_3 fluxes were calculated using observed, bidirectional modeled, and gap-filled fluxes. More than 40% of the total dry NH_3 deposition occurred when air masses were traced back to agricultural source regions. More generally, we identified that 10 (25) more national parks in the U.S. are within 100 (200) km of an NH_3 hotspot, and more observations are needed to quantify the impacts of these hotspots on dry NH_3 deposition in these regions.

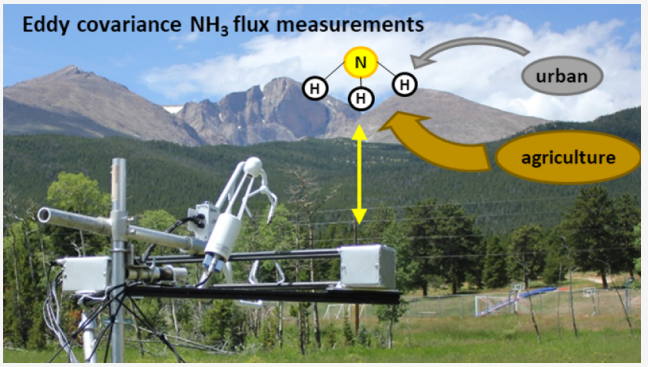

1. INTRODUCTION

Although nitrogen is an essential element for ecosystems, high emissions of anthropogenic reactive nitrogen (N_r), dominated by nitrogen oxides (NO_x) and ammonia (NH_3), adversely impact the environment.[1] For sensitive ecosystems, elevated N_r deposition leads to decreased biological diversity, increased soil acidification, and surface water eutrophication.[2−6] Ellis et al. estimated that in 2006, 24 out of the 45 national parks designated as Class I areas in the contiguous U.S. had excess N_r deposition that could damage their most sensitive ecosystem elements.[7] In recent decades, effective regulations of NO_x emissions in the U.S. and relatively stable NH_3 emissions have led to the increased importance of reduced nitrogen on total N_r deposition.[8] NH_3 dry deposition is estimated to contribute 19−65% of total N_r deposition in different regions in the U.S. for the period of 2011−2013.[8] Observations from ground-based monitoring networks across the U.S. and from satellites in recent decades have shown trends of increasing gas phase NH_3 concentration ranging from 2 to 7% per year.[9,10] If this trend continues, the importance of dry NH_3 deposition is expected to grow. Finally, satellite NH_3 observations have revealed NH_3 emission hotspots with emission rates several orders of magnitude higher than other regions.[11,12] Understanding the impacts of nearby hotspots on dry NH_3 deposition to the sensitive ecosystems can provide critical insights into designing effective mitigation strategies.

Despite the importance of dry NH_3 deposition, observations of NH_3 fluxes in sensitive ecosystems are limited. One area in which the N_r budget has been intensively studied in the U.S. is Rocky Mountain National Park (RMNP) in Colorado, where alpine ecosystems are particularly sensitive to increasing N_r deposition. The eastern edge of RMNP is 80 km away from the maximum of the hotspot located in Weld County, the fourth-highest NH_3 emission hotspot in the U.S.[11,12] Adverse ecological and biogeochemical changes, including elevated surface water nitrate, episodic acidification of surface waters, and changes in diatom species and plant composition, have been

Received: August 26, 2020
Revised: March 31, 2021
Accepted: March 31, 2021
Published: June 1, 2021

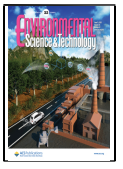

https://doi.org/10.1021/acs.est.0c05749
Environ. Sci. Technol. 2021, 55, 7776−7785

observed in RMNP, especially in the eastern side.[13−15] Multiple studies have been conducted to quantify N_r deposition in the RMNP.[16−21] Due to the scarcity of direct NH_3 flux measurements, dry NH_3 deposition and source attribution for RMNP are usually estimated by model-based methods, which are subject to significant uncertainties because they only partially account for the bidirectional nature of NH_3 flux. At the national scale, although in situ NH_3 observations have become more accessible in recent years, the measurement approaches themselves are not designed for quantifying NH_3 fluxes. Therefore, chemical transport models or inferential methods with in situ or satellite measurements have been used to derive dry NH_3 deposition, which also have large uncertainties.[22]

Major reasons for the lack of direct dry NH_3 deposition measurements, especially in sensitive ecosystems, are the intrinsic challenges associated with using micrometeorological methods.[23] The eddy covariance (EC) method is the most direct, least empirical, and least error-prone approach to measure field-scale integrated exchange flux, but it requires fast response (≥10 Hz) and high-precision NH_3 measurements. Despite the development of high-time resolution NH_3 sensors, including tunable laser spectroscopy and chemical ionization mass spectrometry, conducting EC measurements with a closed-path sensor remains challenging because of the strong surface affinity of NH_3 molecules.[24−28] The adsorption and desorption effects lead to a damping of high-frequency signals. The effects are highly variable depending upon temperature, humidity, cleanliness of the inner surface, the inlet, and the sampling lines.[24,28,29]

In this study, we measured EC NH_3 fluxes in RMNP for two summers using an open-path NH_3 sensor, the first time used in such a low NH_3 environment. We analyzed the EC fluxes in the context of regional transport from local source regions through modeling and in situ measurements. Impacts of transport patterns on dry NH_3 deposition were investigated by comparing cumulative NH_3 fluxes, calculated using modeled and mean diurnal variation (MDV) gap-filled fluxes, for plumes passing through different regions.

2. MATERIALS AND METHODS

2.1. Field Measurements. The open-path quantum cascade (QC) laser-based NH_3 sensor used in this study was a modified version of the sensor that has been deployed on mobile laboratory platforms[30,31] and on an EC measurement tower in a feedlot[32] in northeastern (NE) Colorado. Detailed information about the sensor can be found in Section I of the Supporting Information (SI). In 2015 and 2016, the open-path NH_3 sensor was also installed on an EC measurement tower located south of Estes Park, Colorado (40.28°N, 105.55°W). Wind and temperature were measured using a CSAT3 3D sonic anemometer, and water vapor (H_2O) and carbon dioxide (CO_2) were measured using a LICOR LI-7500 CO_2/H_2O analyzer. Details about the tower setup are provided in Section I of the SI. The measurement system was deployed within a relatively flat grassland area (dominated by *Leucopoa kingii* (Serica watson) W.A. Weber and *Muhlenbergia montana* (Nutt.) Hitchc.) with a canopy height of about 0.3 m and an east-to-west slope of 6.1 ± 0.6% (mean ± 95% confidence interval). The grassland area is surrounded by mixed aspen (*Populus tremuloides* Michx.) and pine (*Pinus latifolia* Sarg.) forest.[33] The EC measurements were conducted from July to August in 2015 and from June to August in 2016. Soil NH_3 emissions from the grassland and the forest areas have been measured with detailed soil information.[33] N_r deposition at the site has been measured annually (3.65 kg N ha^{-1} yr^{-1} in 2009), which includes wet N deposition and dry deposition estimates of nitric acid (HNO_3), NH_3, particulate ammonium (NH_4^+), and particulate nitrate. Dry NH_3 deposition was estimated by multiplying NH_3 concentrations by scaled HNO_3 deposition velocity.[16,19] Measurement methods for other N_r deposition are described by Benedict et al.[19]

In addition to EC measurements, ground-based mobile measurements using the open-path NH_3 sensor and gas-phase NH_3 measurements from a proton-transfer-reaction mass spectrometer (PTR-MS) on the NASA P-3B aircraft[34] during the 2014 DISCOVER-AQ campaign were used to investigate NH_3 transport from source regions to RMNP. Figure S1b shows the setup of the mobile platform, and more details about the observations from 2014 DISCOVER-AQ are provided in Section I of the SI.

2.2. Eddy Covariance Flux. EC fluxes were calculated over 30 min durations following the framework proposed by Mauder et al. with necessary modifications for the open-path NH_3 measurements.[35] High-frequency (10 Hz) data were post-processed, including quality control for all observations and time synchronization for the open-path NH_3 sensor, despiking, and detrending. Then, variances and covariances were calculated and corrected for wind rotation (planar fit), spectral loss due to spatial separation of sensors and path length averaging,[36] H_2O impacts on sonic temperature (SND-correction),[37] density fluctuations (WPL-correction),[38] and spectroscopic corrections.[39] The open-path NH_3 sensor did not measure H_2O concentrations, and LI-7500 H_2O measurements were used for density and spectroscopic corrections. Because the open-path NH_3 sensor had not previously been used to measure low flux over seminatural ecosystems, the random errors (σ) of NH_3 EC flux were calculated to determine the detection limit as 1.96 σ for 95% confidence interval (CI, all uncertainties reported here are 95% CI). In addition, the random errors due to instrumental noise (σ^{instr}) were also estimated to quantify the impacts of sensor performance on flux uncertainty. Cospectra and ogive analyses were also conducted to quantify high-frequency attenuation (HFA) due to sensor separation and path-averaging. More details about EC calculation, random error estimates, and cospectra analyses are provided in Section II of the SI.

Periods with nonideal conditions for the EC method were excluded using quality control filters following the work of Mauder et al., which defined three quality classes.[35] Fluxes in Class 0 are typically used for fundamental research, and fluxes in Class 1 are for long-term data sets.[35] To increase data coverage, especially for upslope events, fluxes in Class 0 and Class 1 were analyzed in this study. Three additional data filters were implemented. First, only measurements with 70% flux occurring within the grassland were used for the following analyses. Footprints of the flux measurements were estimated using the model developed by Kljun et al., and Figure S6 shows the estimated footprints and fetch selections.[40] Second, a frictional velocity (u_*) threshold of 0.05 m s^{-1} was determined based on the assumption that CO_2 flux was invariant with u_* (see Figure S7 for details). Finally, a σ^{instr} threshold of 1 ng NH_3 m^{-2} s^{-1} was implemented to remove periods with inconsistent sensor performance (see Figure S8 for details) caused by reduced mirror reflectivity and optical fringes (constructive and destructive interferences arise from slight reflections among optical components). This requirement filtered out about 10% of the NH_3 flux measurements in 2015, and only two 30-min

https://doi.org/10.1021/acs.est.0c05749
Environ. Sci. Technol. 2021, 55, 7776−7785

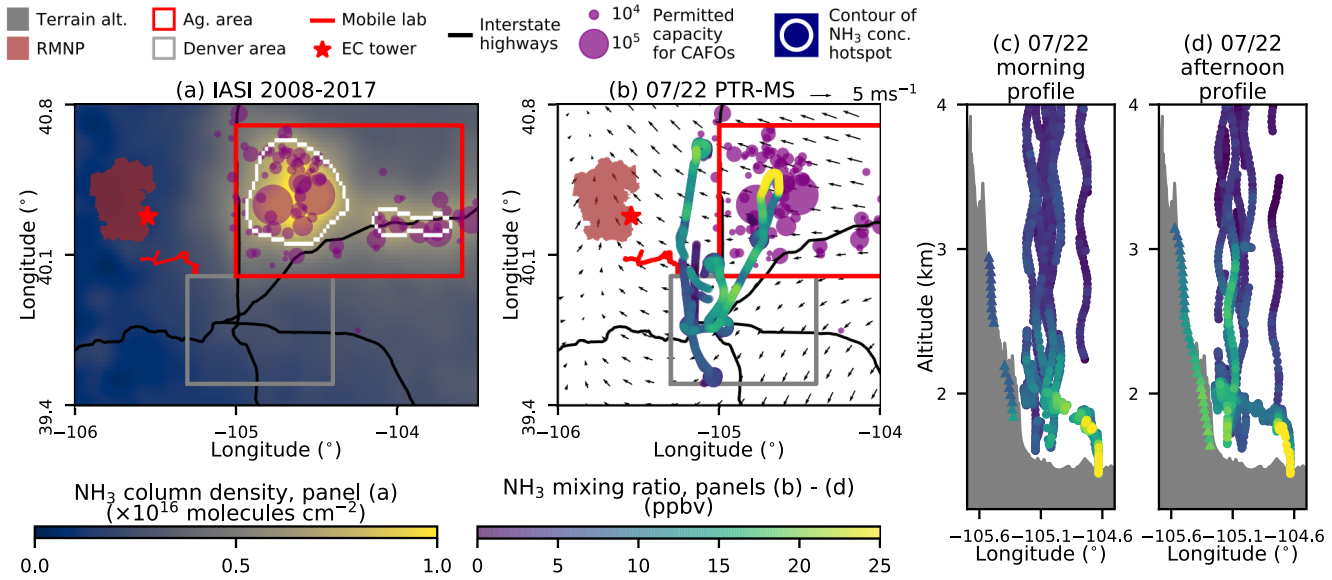

Figure 1. Spatial distributions and vertical profiles of NH_3 observed in northeastern Colorado. Panel (a) shows the IASI annual oversampled NH_3 column density in northeastern Colorado.[43] Panel (b) shows the NH_3 mixing ratios observed by the PTR-MS on the P3-B across northeastern Colorado on July 22nd, 2014 with noontime 10 m wind field. Panels (c) and (d) show the vertical profiles measured by the PTR-MS and the open-path NH_3 sensor on a ground-based mobile platform from 08:00 to 12:00 and from 12:00 to 16:00 local time, respectively. The red star in both (a) and (b) shows the location of the tower site, and the red line shows the driving route of the Princeton Mobile Laboratory on July 22nd, 2014, during the DISCOVER-AQ campaign. The purple circles in panels (a) and (b) show the permitted capacity of concentrated animal feeding operations (CAFOs). The white contours in (a) show the boundaries of concentration hotspots defined as the areas of the 95th percentile of the NH_3 column density in the contiguous U.S. The red and gray boxes show the agricultural (ag) hotspot and the Denver area for trajectory analyses. Circles and triangles in panels (c) and (d) show observations from the PTR-MS and the open-path NH_3 sensor, respectively.

periods were removed in 2016. We kept the measured fluxes below flux detection limits to avoid creating biases as suggested by Langford et al.[41]

In 2015, the sensor had a drifting issue with a time scale of several hours resulting from optical fringes in the system (see Figure S9 for more details). The drifts were removed by a 5 min rolling average detrend. We examined the impact of the drift on flux calculations and found that the influence was negligible after quality control (see Figure S11 and Section III of the SI).

2.3. Trajectory Analyses. In NE Colorado, the metropolitan Denver area and the agricultural (ag) area in the South Platte River valley are the potential source regions that could impact dry NH_3 deposition. Vehicular emissions are a key contributor of NH_3 in the Denver area.[30] Concentrated animal feeding operations (CAFOs) are the dominant sources of NH_3 emissions from the agricultural areas.[42] Satellite NH_3 measurements show large hotspots over the agricultural regions but relatively lower abundances over the Denver area.[43] Golston et al. investigated NH_3 emissions from the CAFOs (dominated by cattle and cows[31]) and found 50% underestimation by the U.S. National Emission Inventory 2014.[31] In addition, during transport to alpine areas, NH_3 emitted from urban and agricultural regions could be deposited along the path or partitioned into particulate NH_4^+ in the aerosol. The impacts of these processes on NH_3 concentrations in RMNP have been investigated by previous studies,[17−19,44] and it has been shown that dry NH_4^+ deposition was about 5−10 times smaller than dry NH_3 deposition from June to August in 2008.[16] Therefore, transport patterns need to be differentiated to understand their impacts. In this study, our goal is to link directly measured dry NH_3 fluxes to transport events on hourly to daily time scales.

Trajectory analyses serve this purpose because they are insensitive to NH_3 emissions and losses along the transport pathways. Twenty four-hour backward trajectories of the air masses originating from 3 m above the tower site were calculated at hourly frequencies in July and August to investigate impacts of NH_3 emitted from Denver and the agricultural hotspot on dry NH_3 deposition in RMNP. The backward trajectories were computed using the HYSPLIT Model (Version 4.0) driven by the three hourly North American Mesoscale model outputs at 12 km grid spacing (NAM12).[45] The trajectories consisted of 24 endpoints corresponding to the air mass location at 1 h intervals and were gridded using Bresenham's line algorithm.[46] Gebhart et al. have shown that the performance of the HYSPLIT Model with NAM12 was similar to a more complicated model.[47] Backward trajectories starting at arrival heights of 3, 10, 50, and 100 m above ground level (agl) were also computed to investigate the influence of starting height (see Section IV of the SI). Measured fluxes were divided into four groups with trajectories passing through (1) only the agricultural area in NE Colorado (defined as the red box in Figure 1a); (2) only the Denver area (defined as the gray box in Figure 1a); (3) both boxes; (4) other regions. Mean values and distributions of the fluxes for different groups were compared to quantify the impacts of different transport patterns on NH_3 flux magnitudes.

2.4. NH_3 Flux Gap-Filling. Trajectory analyses and mean observed flux comparison show how flux magnitudes change with NH_3 transport patterns. However, high-deposition events occur less frequently, and cumulative flux accounts for the frequency differences among the trajectory groups. EC flux measurements are limited to ideal atmospheric conditions, leading to the under-representation of flux during the night and under less turbulent conditions. The cumulative flux calculated using quality-controlled EC fluxes could be biased if there is a strong diurnal pattern. Over seminatural grasslands, equilibria of NH_4^+ and NH_3 in the soils and stomata of the plants are sensitive

https://doi.org/10.1021/acs.est.0c05749
Environ. Sci. Technol. 2021, 55, 7776−7785

to temperature.[48] When the temperature is high, plants and soils could become sources of NH_3 unless NH_3 concentrations near the soils and plants are high enough to suppress the volatilization processes. Soil NH_3 emissions near the site have been quantified by Stratton et al. and showed a strong diurnal pattern.[33] The stomatal transport process of NH_3 is impacted by diurnal patterns of light conditions and temperatures, resulting in higher stomatal conductance during the day.[48,49] Cuticles of the plants are mainly a sink for NH_3, governed by the wetness of the surface, leaf area, and atmospheric chemistry.[48,50] NH_3 deposition during dew formation during the night and re-emission during dew evaporation in the morning were measured at the site by Wentworth et al. in 2015.[51] Because of these factors, a distinct NH_3 flux diurnal pattern is expected, and gap-filling is used to reduce the potential biases of using only quality-controlled EC measurements.

To address the representativeness issue of EC measurements, the bidirectional NH_3 flux model developed by Pleim et al. was used to estimate NH_3 fluxes for periods with NH_3 concentration measurements but for meteorological conditions not ideal for the EC method.[52] The model is a resistance model that includes soil, stomatal, and cuticle fluxes. The model has been incorporated into chemical transport models and has been evaluated for managed fields.[50,52] However, the performance of the model has not been evaluated over seminatural ecosystems such as the site in RMNP. Moreover, the model requires additional observations such as soil and plant emission potentials, soil temperature, and leaf surface pH, which were not directly measured or measured at daily or weekly time scales. Therefore, we also evaluated the model when we had quality-controlled EC NH_3 fluxes. Details of the model, the auxiliary inputs, and the evaluation process are provided in Section V of the SI.

Even with fluxes measured by the EC method and calculated by the bidirectional model, there were still large gaps in the dataset. As the first study to use the open-path NH_3 sensor in a remote area, the sensor did not provide NH_3 concentration measurements all the time because of hardware and software malfunctions and severe weather events. In 2015 and 2016, the gaps for NH_3 concentration measurements were 55 and 39% of the campaign periods, respectively. Therefore, the mean diurnal variation (MDV) method, which interpolates the missing NH_3 flux for a certain 30-min period by the average of observed and modeled NH_3 fluxes at the same time of day, was used to fill the periods without NH_3 flux measurements or NH_3 concentrations for simulation. Moffat et al. showed that this method had a moderate but consistent performance for net ecosystem CO_2 exchange, which also has a distinct flux diurnal pattern.[53] However, Flechard et al. have shown that using MDV for NH_3 flux may lead to large uncertainty.[54] The nighttime deposition from the EC measurements could be overestimated because low-turbulence periods are removed, and, thus, both observed and simulated fluxes are used to derive the MDV.

The uncertainties of the gap-filled fluxes by the bidirectional model and the MDV method were estimated differently. The errors of the model fluxes were estimated using hourly composited diurnal root-mean-square deviations (RMSD) between measured and modeled fluxes. The error changes throughout the day because the model performance may vary under different conditions. The errors of the MDV gap-filled fluxes were estimated using hourly composited diurnal standard deviations (SD) of the measured and modeled NH_3 fluxes. When calculating the cumulative flux, the errors of measured, modeled, and MDV gap-filled fluxes were assumed to be Gaussian and independent. More details about the error estimation are in Section VI of the SI.

3. RESULTS

3.1. NH_3 Transport during an Upslope Event. In NE Colorado, there is a terrain-driven, diurnal wind flow pattern when synoptic-scale influences are weak.[55] During the nighttime and in the early morning, higher radiative cooling in the mountain area causes downslope airflows to the plains. During the day, terrain heating leads to reverse upslope flows, and transport is generally from the plains to the higher terrain. An upslope event occurred on July 22nd, 2014 that was sampled well by aircraft over the plains and by the mobile laboratory in the mountains. Figure S6a−c shows the surface winds and surface temperature on July 22nd, 2014 obtained from the NAM12.[45] The daytime flow pattern can be weakened by cloud cover and synoptic-scale winds, leading to a hybrid pattern, where thermally driven upslope flow is more pronounced in the mountain areas, and synoptic-scale flow has a greater influence over the plains. Such a pattern was observed on July 31st, 2014 as wind fields shown in Figure S4d−f and is another relevant case study.

As shown in Figure 1b, NH_3 emitted from the agriculture region was transported to the mountains during the upslope event on July 22nd, 2014. Significant increases of NH_3 throughout the vertical profile in the mountains were observed by the open-path NH_3 sensor and the PTR-MS as the upslope event developed in the afternoon on July 22nd, 2014 (Figure 1c,d). NH_3 concentrations increased by 4.3 ± 1.2 ppbv from early morning to late afternoon at 2.9 km above the sea level (asl). At 2.5 and 2.0 km asl, NH_3 increased by 6.4 ± 2.6 and 11.8 ± 5.2 ppbv, respectively, from 9:30 to 17:00. In contrast to the upslope event on July 22nd, 2014, NH_3 concentrations observed near the RMNP were significantly lower on July 31st, 2014, as shown in Figure S5. The results from PTR-MS also showed that NH_3 concentrations were lower than that on July 22nd, 2014 over the NE Colorado areas. The case studies during DISCOVER-AQ demonstrate that NH_3 is readily transported to the site during upslope flow.

3.2. NH_3 Eddy Covariance Measurements. *3.2.1. Sensor and Eddy Covariance Performance.* The 10 Hz precision of the open-path NH_3 sensor was around 0.1 ppbv during the field campaign. NH_3 concentration measurements were compared with an annular denuder and a filter pack (URG Corporation, Chapel Hill, NC) near the site on a daily scale and showed relatively good agreement (a slope of 0.75 ± 0.16 and an intercept of −0.03 ± 0.13 ppbv using orthogonal regression with an R^2 of 0.61, see Figure S10). Defining flux detection limit as 1.96σ, the median detection limits were around 2.2 and 1.9 ng NH_3 m^{-2} s^{-1} in 2015 and 2016, respectively, which were comparable to the detection limit of 2.15 ng NH_3 m^{-2} s^{-1} reported for a closed-path instrument with similar 10 Hz precision.[28] This flux detection limit in 2016 is 100% (220%) larger than the median (mean) absolute NH_3 flux, and 16 and 21% of the quality-controlled NH_3 flux measurements were below the detection limit in 2015 and 2016, respectively. The fluxes below the flux detection limit were included in our analyses to prevent a positive bias.[41] The average NH_3 flux losses due to high-frequency attenuation (HFA) over the measurement periods in 2015 and 2016 were estimated to be 10 and 7% using the Ogive method proposed by Ammann et al.[56] The flux loss due to HFA is similar to the flux loss reported by Sun et al.

https://doi.org/10.1021/acs.est.0c05749
Environ. Sci. Technol. 2021, 55, 7776−7785

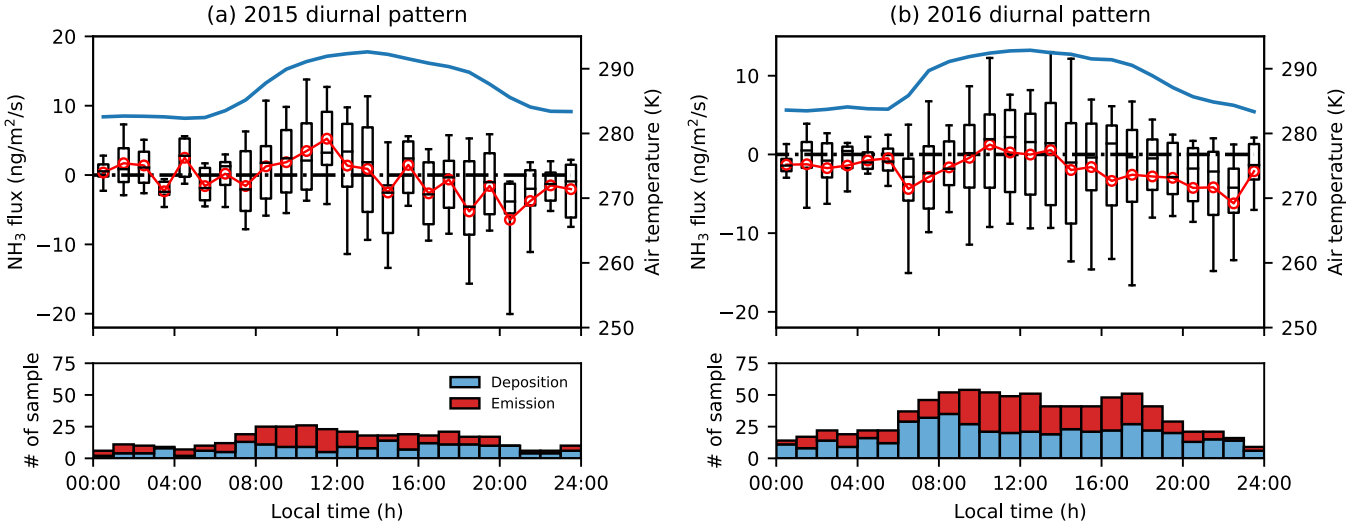

Figure 2. Hourly composite NH_3 fluxes and hourly mean air temperatures observed in (a) 2015 and (b) 2016. The boxes and whiskers represent 10th, 25th, 50th, 75th, and 90th percentiles of hourly composite data. The red circles and the red lines show hourly mean fluxes. The blue lines in the top panels show hourly mean temperatures. The blue and red bars in the bottom panels indicate numbers of samples of positive and negative fluxes, respectively.

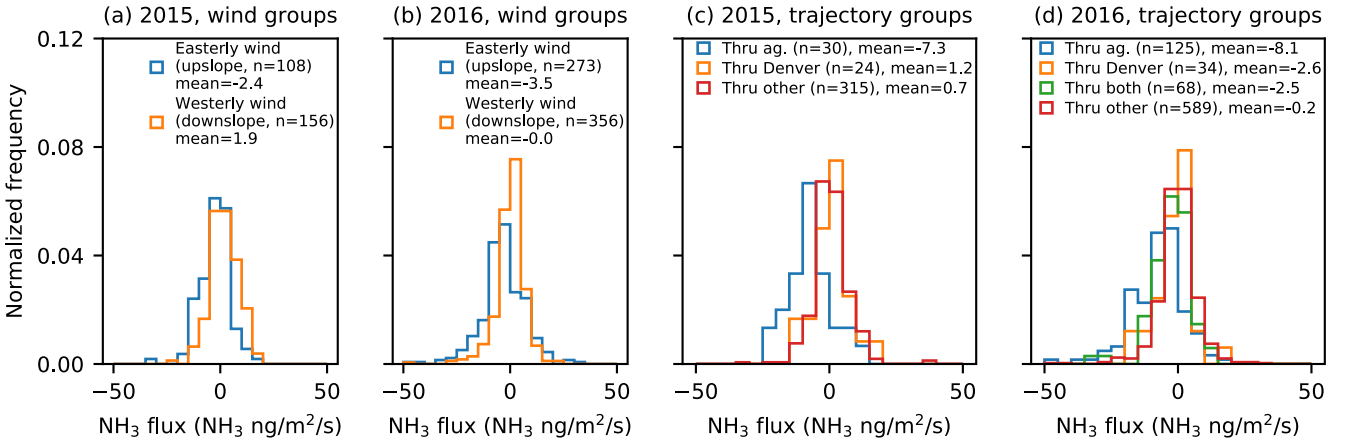

Figure 3. Histograms of observed NH_3 flux for different wind directions observed in (a) 2015 and (b) 2016 and different trajectories in (c) 2015 and (d) 2016. In 2015, only three 30-min periods had trajectories through both agricultural (ag) and Denver areas and are not shown in panel (c).

and is significantly better than about 40% loss rates reported by Whitehead et al. and Moravek et al. using closed-path laser-based sensors.[25,28,32] More details can be found in Section III of the SI.

3.2.2. Observed NH_3 Flux. With all of the filters applied, quality-controlled EC flux measurements accounted for 32 and 39% of daytime fluxes and 17 and 17% of nighttime fluxes for NH_3 in 2015 and 2016, respectively (Table S4). Both deposition and emission events were observed with a strong diurnal pattern. Composite diurnal variation curves of NH_3 flux using quality-controlled EC flux measurements are presented in Figure 2. Measurements made between August 19th, 2015 and August 25th, 2015 were impacted by wildfire plumes. Although wildfire impacts on dry NH_3 deposition is an important topic,[57] the single event might not be proportionally represented compared to the short duration of the 2015 field campaign. Therefore, results from this period were excluded from the following analyses. More details can be found in Section VII of the SI.

The hourly composite NH_3 fluxes show net deposition in the early morning and from late afternoon to midnight. Net emissions were observed in the morning, which might be related to soil emissions and dew evaporation events, as reported by Wentworth et al.[51] The dew study and this study were not coordinated, and therefore, only two of the events reported by Wentworth et al. for the same site were also partially captured by the EC flux. A strong morning emission (5.3 ng NH_3 m^{-2} s^{-1} from 07:00 to 10:00) was observed on July 22nd, 2015 but there was no EC measurement the previous night. On July 28th, 2015, a strong late-night deposition was observed (mean (minimum) flux of −4.9 (−10.0) ng NH_3 m^{-2} s^{-1} from 09:00 to 12:00), but no re-emission the next morning (mean flux of 0.1 ng NH_3 m^{-2} s^{-1} from 07:00 to 10:00). Specific studies designed for comparing dew formation and evaporation-related NH_3 flux and EC measured flux are needed.

In addition to the diurnal pattern, NH_3 flux patterns were also linked to wind directions. Blue and orange areas in Figure S19 represent periods with westerly (downslope) and southeasterly (upslope) winds, respectively. The winds measured at 10 m agl from the nearby CASTNET site were used to minimize local terrain and forest impacts on airflow. Figure 3a,b shows histograms of quality-controlled daytime NH_3 fluxes (06:00 to 20:00) with different wind directions for 2015 and 2016, respectively. Daytime fluxes were used for the analyses to reduce the impact of wind diurnal patterns and because nighttime winds

https://doi.org/10.1021/acs.est.0c05749
Environ. Sci. Technol. 2021, 55, 7776−7785

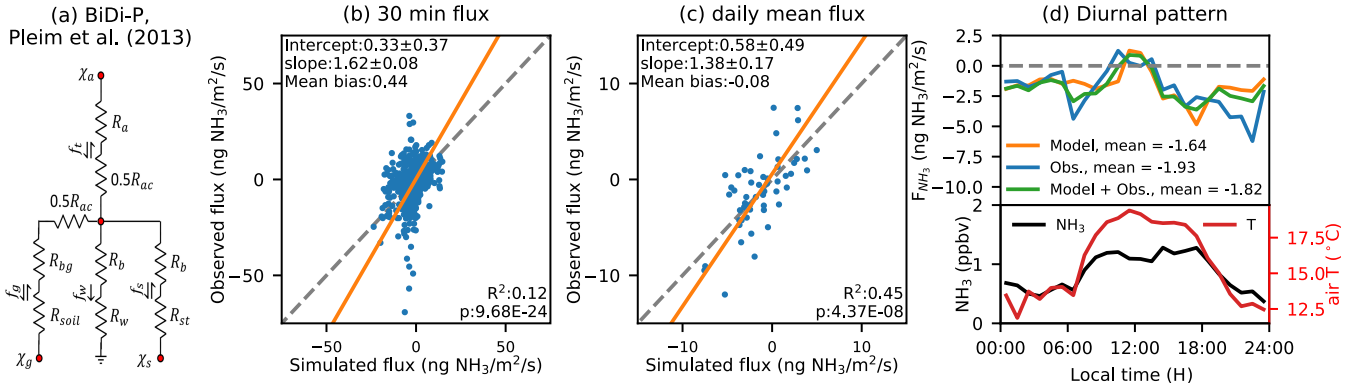

Figure 4. Comparison between observed and modeled NH_3 fluxes. Panel (a) shows schematic diagram of the bidirectional model. χ_a is the ambient NH_3 concentration, and χ_g and χ_s are the soil and stomatal compensation points, respectively. R_a, R_b, R_{ac}, R_{bg}, R_{soil}, R_w, and R_{st} are aerodynamic, quasi-laminar boundary layer, in-canopy, ground quasi-laminar boundary layer, in-soil, cuticle, and stomatal resistances, respectively. f_t, f_g, f_w, and f_s are total exchange, ground, cuticle, and stomatal NH_3 fluxes, respectively. Details of the model are provided in Section V of the SI. Panels (b) and (c) compare the observed and modeled NH_3 fluxes on 30-min and daily time scales, respectively. The orange lines show orthogonal regression results. Panel (d) shows the comparison for hourly composite diurnal means of observed (blue), modeled (orange), and both observed and modeled (green) fluxes along with the diurnal NH_3 mixing ratio (black) and temperature (red) variations.

near the surface may be decoupled with the large-scale flow pattern. The mean NH_3 fluxes with westerly winds were 1.9 and 0 ng NH_3 m^{-2} s^{-1} in 2015 and 2016, respectively. The mean NH_3 fluxes with easterly winds were −2.4 and −3.5 ng NH_3 m^{-2} s^{-1} in 2015 and 2016, respectively. Although the mean fluxes were close to or below the estimated detection limit for the 30-min flux period, the majority of the flux measurements were above the detection limit, and averaging them reduces their random errors. Figure S10a,b shows the time series of observed NH_3 during relatively stable periods and corresponding Allan deviation analyses.

Welch's *t*-test (two-sided) was conducted using quality-controlled EC fluxes to check if the differences were statistically significant using Statsmodels.[58] For both 2015 and 2016, the differences in NH_3 and H_2O fluxes between different wind groups were statistically significant ($p < 0.05$), whereas the differences in sensible heat and CO_2 fluxes were not (see Table S9 for more details). This result indicates that the differences in H_2O and NH_3 fluxes between different wind direction groups might be related to large-scale transport events. Figure S21 shows the averaged NAM surface temperature and surface wind field for the periods with high emission and high deposition. The mean surface temperature was higher for the periods with observed high emissions compared to the periods with high deposition. Upslope winds capable of transporting NH_3 emissions from NE Colorado into RMNP were observed, while no consistent wind pattern was found for the periods with high local emissions.

Although the wind group analyses show a strong dependence of NH_3 flux on wind direction, such an analysis does not distinguish the sources in Colorado. To quantify mean NH_3 flux for periods with plumes coming from different regions, the observed fluxes were grouped as described in Section 2.3. Figure 3c,d shows histograms of NH_3 flux for the four groups in 2015 and 2016, respectively. Table S5 lists frequencies of the four groups for July and August and for periods with quality-controlled EC observations. The spatial distributions of the trajectories are shown in Figure S15. The average NH_3 fluxes were −7.3 and −8.1 ng NH_3 m^{-2} s^{-1} during the periods with trajectories only passing through the agricultural area in NE Colorado in 2015 and 2016, respectively. These deposition rates were consistently higher than other trajectory groups in both years. For periods with trajectories passing through only Denver, there were slight net emissions in 2015 (1.2 ng NH_3 m^{-2} s^{-1}) but deposition in 2016 (−2.6 ng NH_3 m^{-2} s^{-1}). The difference between 2015 and 2016 for the Denver only trajectory group is likely caused by the large data gap of 2015 observations. The hybrid cases had similar net deposition to that of the Denver area in 2016, which indicates a fraction of NH_3 may have partitioned to particulate NH_4^+ when passing through only the Denver area. The observation in 2015 only had three 30-min observations for the hybrid cases ($n = 3$; mean flux, −7.9 ng NH_3 m^{-2} s^{-1}), and, therefore, are not shown in Figure 3c. When the air masses did not pass through these regions, there were small emissions of 0.7 ng NH_3 m^{-2} s^{-1} in 2015, and deposition and emissions were balanced in 2016.

3.3. Modeled NH_3 Flux. NH_3 fluxes in 2016 simulated by the bidirectional NH_3 flux model (Figure 4a shows a schematic diagram of the model) were compared with the quality-controlled NH_3 flux observations. Figure 4b shows the comparison for 30-min NH_3 fluxes, and the model performed moderately with an R^2 of 0.12 and underestimated the variability of NH_3 flux by about 60%. On a daily scale, the model showed a better agreement (R^2 = 0.45) but still underestimated the variability of NH_3 flux (Figure 4c). Figure 4d shows the diurnal pattern of the fluxes modeled by the bidirectional models, as well as that of the observed fluxes. The bidirectional flux model failed to reproduce late-night and early morning deposition and the emission peak in the morning. These discrepancies might be related to emission mechanisms that are not included in current bidirectional models, such as the influence of dew formation and evaporation on NH_3 fluxes.[51] Also, the nighttime EC flux could be biased toward high-turbulence conditions, causing the discrepancies. Removing the turbulence-condition quality control leads to a better agreement between the daily means and the diurnal patterns of observed and modeled NH_3 fluxes, especially during the night (see Figure S17).

Besides potential EC measurement and model errors, the large uncertainties of input data may cause the discrepancies. First, the air temperature was used to approximate soil and stomata temperatures, which could differ in their diurnal patterns. Second, the emission potentials of stomata and soil were assumed to be constant. Previous studies have shown that both the amount of dissolved ammonium [NH_4^+] and the pH of

https://doi.org/10.1021/acs.est.0c05749
Environ. Sci. Technol. 2021, 55, 7776−7785

the soil or the leaf stomata may change significantly, but their diurnal variabilities and associated drivers are not well understood.[21] Finally, several needed inputs, such as leaf surface pH, which was approximated using wet deposition pH, were only available at daily to weekly time scales. The large uncertainties of input data also limit our capability in optimizing the model as it is hard to distinguish the errors caused by input uncertainties and model errors.

Figures S18 and S19 compare hourly composite NH_3 flux for all quality-controlled EC fluxes and modeled fluxes group by wind directions and trajectories, respectively, along with model errors, SD for the MDV method, diurnal variations of temperature and NH_3 mixing ratios, and frequencies of associated flux events. Nighttime deposition of quality-controlled EC fluxes is typically higher than that of modeled fluxes in these cases. However, it is hard to quantify whether the differences are caused by the aforementioned model and input errors or the potential overestimations of nighttime flux of the quality-controlled EC fluxes. To reduce the impacts of nighttime NH_3 flux uncertainty on the cumulative flux, the MDV for gap-filling is derived using both observed and modeled NH_3 fluxes (green line in Figure 4d).

3.4. Cumulative NH_3 Flux. The total cumulative dry NH_3 depositions for July and August in 2016 were estimated to be 83 ± 18 g N ha^{-1} using observed, modeled, and MDV gap-filled NH_3 fluxes, which is 50% of the value (173 g N ha^{-1}) estimated using the inferential method proposed by Benedict et al.[16] Because of the drifting issue and large data gaps, we did not estimate cumulative flux in 2015. Dry NH_3 deposition accounted for around 12% of the total N_r deposition and contributed around 41% of dry N_r deposition for July and August in 2016.

Although the mean deposition rate with trajectories passing through only the agricultural hotspot was significantly higher than other groups, the frequency of such events was low (12−14%). Cumulative NH_3 fluxes that occurred during periods with different trajectory groups account for this aspect. Cumulative fluxes calculated using quality-controlled EC, modeled, and MDV gap-filled fluxes are presented here. Results based on quality-controlled EC fluxes alone and both EC and modeled fluxes are provided in Table S7. Cumulative fluxes for periods with different trajectories vary with starting heights of backward trajectories (see Table S7), and the mean values of trajectories starting from 3, 10, 50, and 100 m are discussed here. The cumulative NH_3 deposition during periods with trajectories passing through only the agricultural hotspot was 33 ± 8 g N ha^{-1}, about 39 ± 4% of the total cumulative NH_3 flux. The cumulative NH_3 depositions during periods with trajectories passing through only the Denver area and through both regions in 2016 were about 8 ± 4 and 10 ± 3 g N ha^{-1}, respectively, accounting for 10 ± 4 and 12 ± 3% of total dry NH_3 deposition in July and August. Cumulative flux for periods with trajectories from regions other than Denver and agricultural areas in NE Colorado was about 31 ± 11 g N ha^{-1} (38 ± 6% of total cumulative flux).

Thompson et al. estimated that the sources within Colorado contributed only 29% of the annual dry NH_3 deposition for the same observation site using a chemical transport model.[44] In our analyses, the cumulative NH_3 fluxes with trajectories passing through the agricultural or urban regions may also be impacted by other upwind NH_3 sources, reducing their contribution to total dry NH_3 deposition. However, the trajectories passing through urban and agricultural regions had similar patterns before passing through these two regions. Yet, the flux difference was significant in both 2015 and 2016, indicating that the high deposition associated with agricultural area only trajectory was not caused by upwind regions. Since we only measured NH_3 fluxes from June to August, seasonality may lead to the difference. Another potential cause of the difference is that the model used by Thompson et al. did not take the bidirectional nature of NH_3 flux into account.[44] The simulated NH_3 flux would always be negative, and the small negative fluxes with high occurrence would appear to have a larger contribution to the total dry NH_3 deposition. Finally, our estimate was for grasslands or open fields in RMNP, whereas the estimate from Thompson et al. was for the whole RMNP.[44]

4. DISCUSSION

Using our mobile measurements during the 2014 DISCOVER-AQ campaign, we demonstrated the evolution of an upslope event that transported NH_3 emissions from NE Colorado to the RMNP area. Subsequently, the transported NH_3 during such events leads to a significant increase in dry NH_3 deposition. In 2015 and 2016, we demonstrated the capability of the open-path NH_3 sensor to measure EC NH_3 flux in a remote area with a low detection limit of 2 ng NH_3 m^{-2} s^{-1}. Grouping the observed EC NH_3 fluxes by wind directions, we found that NH_3 deposition was generally associated with easterly wind during the daytime, indicating large impacts of hotspot NH_3 emissions. We showed that dry NH_3 deposition during the periods with a backward trajectory passing through just the agricultural regions in NE Colorado was significantly higher than periods with the air mass coming from other regions. Cumulative deposition from air masses transiting the emissions from the hotspot in the agricultural region accounted for more than 40% of the total dry NH_3 deposition, including trajectories that passed through only the agricultural region and both agricultural and Denver areas, in the summer of 2016.

Combining wet and dry N_r deposition, we estimated the total N_r deposition rates at the site for July and August to 716 ± 61 g N ha^{-1} in 2016, respectively. We estimated that dry NH_3 contributed around 12% of the total deposition in July and August in 2016, respectively. These deposition rates represent NH_3 fluxes just over grasslands in RMNP. Stratton et al. reported that soil emissions from grasslands in RMNP (3.0 ng NH_3 m^{-2} s^{-1}) were 150% higher than those from forests (1.2 ng NH_3 m^{-2} s^{-1}).[33] The difference between the soil emissions from grasslands and forests is similar to the mean net NH_3 flux measured (−2.0 ng NH_3 m^{-2} s^{-1}) at the site in 2016. Furthermore, the larger leaf area and the higher roughness above the forest canopy favor NH_3 deposition. Therefore, NH_3 deposition over RMNP forests may be significantly higher than the results reported for grasslands in this study. More observations are needed to investigate dry NH_3 flux patterns over different underlying ecosystems. Moreover, our observations were limited to summer, and NH_3 flux observations in other seasons are needed to constrain the annual dry deposition flux of NH_3 as well as the influence of emissions from the emission hotspots. Finally, gap-filling using the bidirectional model and the MDV method may have systematic biases that are not included in our uncertainty estimates, especially during the nighttime with limited samples for specific conditions. Further evaluation and optimization of the bidirectional model and development of the gap-filling method for NH_3 flux are needed. Despite having a comprehensive suite of observations at the site, we encountered significant challenges acquiring inputs for the

https://doi.org/10.1021/acs.est.0c05749
Environ. Sci. Technol. 2021, 55, 7776−7785

bidirectional model, such as soil pH, soil water content, and leaf pH. This issue would be more pronounced and lead to a larger uncertainty in other regions with limited data availability and should be considered in the experimental design for future evaluation studies.

Although there are several limiting factors of this study, we linked directly measured NH_3 deposition with the transport pattern bringing NH_3 emissions from the agricultural region to RMNP. Our results indicate that mitigating the hotspot NH_3 emissions near RMNP with local initiatives and emission reduction programs could be an effective way to reduce dry NH_3 deposition in RMNP. In addition, NH_3 transported from agricultural hotspots may contribute to wet deposition through washout and particulate NH_4^+ deposition. Other national parks and wilderness areas could potentially be impacted by U.S. NH_3 emission hotspots (as shown in Figure S22 and listed in Table S10), and very limited observations are available for those regions. The method demonstrated in this study could be implemented in the future to quantify dry NH_3 flux and potential impacts from NH_3 emission or concentration hotspots.

■ ASSOCIATED CONTENT

Supporting Information

The Supporting Information is available free of charge at https://pubs.acs.org/doi/10.1021/acs.est.0c05749.

Supplementary figures and tables; descriptions of instruments; eddy covariance calculation; trajectory analyses; bidirectional ammonia flux model; uncertainty estimation; and national park near ammonia hotspots (PDF)

■ AUTHOR INFORMATION

Corresponding Author

Mark A. Zondlo − *Department of Civil and Environmental Engineering, Princeton University, Princeton 08544, New Jersey, United States; Center for Mid-Infrared Technologies for Health and the Environmental, NSF-ERC, Princeton, New Jersey 08540, United States;* orcid.org/0000-0003-2302-9554; Phone: 609-258-5037; Email: mzondlo@princeton.edu; Fax: 609-258-2799

Authors

Da Pan − *Department of Civil and Environmental Engineering, Princeton University, Princeton 08544, New Jersey, United States; Center for Mid-Infrared Technologies for Health and the Environmental, NSF-ERC, Princeton, New Jersey 08540, United States*

Katherine B. Benedict − *Department of Atmospheric Science, Colorado State University, Fort Collins, Colorado 80523, United States*

Levi M. Golston − *Department of Civil and Environmental Engineering, Princeton University, Princeton 08544, New Jersey, United States; Center for Mid-Infrared Technologies for Health and the Environmental, NSF-ERC, Princeton, New Jersey 08540, United States;* Present Address: Atmospheric Science Branch, NASA Ames Research Center, Moffett Field, California 94035-1000, United States.

Rui Wang − *Department of Civil and Environmental Engineering, Princeton University, Princeton 08544, New Jersey, United States; Center for Mid-Infrared Technologies for Health and the Environmental, NSF-ERC, Princeton, New Jersey 08540, United States*

Jeffrey L. Collett, Jr − *Department of Atmospheric Science, Colorado State University, Fort Collins, Colorado 80523, United States*

Lei Tao − *Department of Civil and Environmental Engineering, Princeton University, Princeton 08544, New Jersey, United States; Center for Mid-Infrared Technologies for Health and the Environmental, NSF-ERC, Princeton, New Jersey 08540, United States*

Kang Sun − *Department of Civil, Structural and Environmental Engineering, University at Buffalo, Buffalo, New York 14260, United States; Research and Education in Energy, Environment and Water (RENEW) Institute, University at Buffalo, Buffalo, New York 14260, United States*

Xuehui Guo − *Department of Civil and Environmental Engineering, Princeton University, Princeton 08544, New Jersey, United States; Center for Mid-Infrared Technologies for Health and the Environmental, NSF-ERC, Princeton, New Jersey 08540, United States*

Jay Ham − *Department of Soil and Crop Sciences, Colorado State University, Fort Collins, Colorado 80521, United States*

Anthony J. Prenni − *Air Resources Division, National Park Service, Lakewood, Colorado 80235, United States*

Bret A. Schichtel − *Air Resources Division, National Park Service, Fort Collins, Colorado 80525, United States*

Tomas Mikoviny − *Chemistry and Dynamics Branch, Science Directorate, NASA Langley Research Center, Hampton, Virginia 23666, United States; Oak Ridge Associated Universities, Oak Ridge, Tennessee 37830, United States; Department of Chemistry, University of Oslo, Oslo 0315, Norway*

Markus Müller − *Institute for Ion Physics and Applied Physics, University of Innsbruck, Innsbruck 6020, Austria;* Present Address: Ionicon Analytik, Innsbruck 6020, Austria.

Armin Wisthaler − *Department of Chemistry, University of Oslo, Oslo 0315, Norway; Institute for Ion Physics and Applied Physics, University of Innsbruck, Innsbruck 6020, Austria;* orcid.org/0000-0001-5050-3018

Complete contact information is available at: https://pubs.acs.org/10.1021/acs.est.0c05749

Author Contributions

The manuscript was written through contributions of all authors. All authors have given approval to the final version of the manuscript.

Notes

The authors declare no competing financial interest.

Data availability: Mobile measurements and 30-min eddy covariance fluxes are publicly available at https://doi.org/10.34770/h7as-r856. Raw 10-Hz observations used for flux calculation are available upon request from the corresponding author.

■ ACKNOWLEDGMENTS

D.P. and L.M.G. acknowledge support for the DISCOVER-AQ field measurements from NASA NNX14AT36G/NNX14AT32G. X.G. acknowledges support from a NASA Earth and Space Science Fellowship NASA 80NSSC17K0377. Satellite analyses were supported by NASA NNX16AQ90G. The authors acknowledge Lars Wendt, Victor Fu, Naomi Pohl, and Levi Stanton for their assistance with the Princeton field data collection in Colorado. The authors appreciate the NASA DISCOVER-AQ science team and aircraft and technical crews.

PTR-MS measurements during DISCOVER-AQ were supported by the Austrian Federal Ministry for Transport, Innovation and Technology (BMVIT) through the Austrian Space Applications Programme (ASAP 8, #833451 and #840086) of the Austrian Research Promotion Agency (FFG). Measurements in RMNP were supported by the National Park Service and USEPA. The assumptions, findings, conclusions, judgments, and views presented herein are those of the authors and should not be interpreted as necessarily representing the National Park Service.

REFERENCES

(1) Galloway, J. N.; Townsend, A. R.; Erisman, J. W.; Bekunda, M.; Cai, Z.; Freney, J. R.; Martinelli, L. A.; Seitzinger, S. P.; Sutton, M. A. Transformation of the nitrogen cycle: recent trends, questions, and potential solutions. *Science* **2008**, *320*, 889−892.

(2) Clark, C. M.; Tilman, D. Loss of plant species after chronic low-level nitrogen deposition to prairie grasslands. *Nature* **2008**, *451*, 712−715.

(3) Phoenix, G. K.; Emmett, B. A.; Britton, A. J.; Caporn, S. J.; Dise, N. B.; Helliwell, R.; Jones, L.; Leake, J. R.; Leith, I. D.; Sheppard, L. J. Impacts of atmospheric nitrogen deposition: responses of multiple plant and soil parameters across contrasting ecosystems in long-term field experiments. *Global Change Biol.* **2012**, *18*, 1197−1215.

(4) Holtgrieve, G. W.; Schindler, D. E.; Hobbs, W. O.; Leavitt, P. R.; Ward, E. J.; Bunting, L.; Chen, G.; Finney, B. P.; Gregory-Eaves, I.; Holmgren, S. A coherent signature of anthropogenic nitrogen deposition to remote watersheds of the northern hemisphere. *Science* **2011**, *334*, 1545−1548.

(5) Janssens, I.; Dieleman, W.; Luyssaert, S.; Subke, J.-A.; Reichstein, M.; Ceulemans, R.; Ciais, P.; Dolman, A. J.; Grace, J.; Matteucci, G. Reduction of forest soil respiration in response to nitrogen deposition. *Nat. Geosci.* **2010**, *3*, 315−322.

(6) Zhan, X.; Bo, Y.; Zhou, F.; Liu, X.; Paerl, H. W.; Shen, J.; Wang, R.; Li, F.; Tao, S.; Dong, Y.; Tang, X. Evidence for the Importance of Atmospheric Nitrogen Deposition to Eutrophic Lake Dianchi, China. *Environ. Sci. Technol.* **2017**, *51*, 6699−6708.

(7) Ellis, R.; Jacob, D. J.; Sulprizio, M. P.; Zhang, L.; Holmes, C.; Schichtel, B.; Blett, T.; Porter, E.; Pardo, L.; Lynch, J. Present and future nitrogen deposition to national parks in the United States: critical load exceedances. *Atmos. Chem. Phys.* **2013**, *13*, 9083−9095.

(8) Li, Y.; Schichtel, B. A.; Walker, J. T.; Schwede, D. B.; Chen, X.; Lehmann, C. M.; Puchalski, M. A.; Gay, D. A.; Collett, J. L. Increasing importance of deposition of reduced nitrogen in the United States. *Proc. Natl. Acad. Sci. U.S.A.* **2016**, *113*, No. 201525736.

(9) Butler, T.; Vermeylen, F.; Lehmann, C.; Likens, G.; Puchalski, M. Increasing ammonia concentration trends in large regions of the USA derived from the NADP/AMoN network. *Atmos. Environ.* **2016**, *146*, 132−140.

(10) Warner, J. X.; Wei, Z.; Strow, L. L.; Dickerson, R. R.; Nowak, J. B. The global tropospheric ammonia distribution as seen in the 13-year AIRS measurement record. *Atmos. Chem. Phys.* **2016**, *16*, 5467.

(11) van Damme, M.; Clarisse, L.; Whitburn, S.; Hadji-Lazaro, J.; Hurtmans, D.; Clerbaux, C.; Coheur, P.-F. Industrial and agricultural ammonia point sources exposed. *Nature* **2018**, *564*, 99−103.

(12) Dammers, E.; Mclinden, C. A.; Griffin, D.; Shephard, M. W.; Van Der Graaf, S.; Lutsch, E.; Schaap, M.; Gainairu-Matz, Y.; Fioletov, V.; Van Damme, M. NH3 emissions from large point sources derived from CrIS and IASI satellite observations. *Atmos. Chem. Phys.* **2019**, *19*, 12261−12293.

(13) Baron, J. S.; Driscoll, C. T.; Stoddard, J. L.; Richer, E. E. Empirical Critical Loads of Atmospheric Nitrogen Deposition for Nutrient Enrichment and Acidification of Sensitive US Lakes. *BioScience* **2011**, *61*, 602−613.

(14) Bowman, W. D.; Murgel, J.; Blett, T.; Porter, E. Nitrogen critical loads for alpine vegetation and soils in Rocky Mountain National Park. *J. Environ. Manage.* **2012**, *103*, 165−171.

(15) Burns, D. A. The effects of atmospheric nitrogen deposition in the Rocky Mountains of Colorado and southern Wyoming, USA—a critical review. *Environ. Pollut.* **2004**, *127*, 257−269.

(16) Benedict, K. B.; Carrico, C. M.; Kreidenweis, S. M.; Schichtel, B.; Malm, W.; Collett, J. L. A seasonal nitrogen deposition budget for Rocky Mountain National Park. *Ecol. Appl.* **2013**, *23*, 1156−1169.

(17) Benedict, K. B.; Day, D.; Schwandner, F. M.; Kreidenweis, S. M.; Schichtel, B.; Malm, W. C.; Collett, J. L., Jr Observations of atmospheric reactive nitrogen species in Rocky Mountain National Park and across northern Colorado. *Atmos. Environ.* **2013**, *64*, 66−76.

(18) Li, Y.; Thompson, T. M.; Damme, M. V.; Chen, X.; Benedict, K. B.; Shao, Y.; Day, D.; Boris, A.; Sullivan, A. P.; Ham, J. Temporal and spatial variability of ammonia in urban and agricultural regions of northern Colorado, United States. *Atmos. Chem. Phys.* **2017**, *17*, 6197−6213.

(19) Benedict, K. B.; Prenni, A. J.; Sullivan, A. P.; Evanoski-Cole, A. R.; Fischer, E. V.; Callahan, S.; Sive, B. C.; Zhou, Y.; Schichtel, B. A.; Collett, J. L., Jr Impact of Front Range sources on reactive nitrogen concentrations and deposition in Rocky Mountain National Park. *PeerJ* **2018**, *6*, No. e4759.

(20) Beem, K. B.; Raja, S.; Schwandner, F. M.; Taylor, C.; Lee, T.; Sullivan, A. P.; Carrico, C. M.; McMeeking, G. R.; Day, D.; Levin, E. Deposition of reactive nitrogen during the Rocky Mountain Airborne Nitrogen and Sulfur (RoMANS) study. *Environ. Pollut.* **2010**, *158*, 862−872.

(21) Hrdina, A.; Moravek, A.; Schwartz-Narbonne, H.; Murphy, J. Summertime Soil-Atmosphere Ammonia Exchange in the Colorado Rocky Mountain Front Range Pine Forest. *Soil Syst.* **2019**, *3*, No. 15.

(22) Walker, J. T.; Beachley, G.; Zhang, L.; Benedict, K. B.; Sive, B. C.; Schwede, D. B. A review of measurements of air-surface exchange of reactive nitrogen in natural ecosystems across North America. *Sci. Total Environ.* **2020**, *698*, No. 133975.

(23) Zhang, L.; Wright, L.; Asman, W. Bi-directional air-surface exchange of atmospheric ammonia: A review of measurements and a development of a big-leaf model for applications in regional-scale air-quality models. *J. Geophys. Res.: Atmos.* **2010**, *115*, No. 13589.

(24) Sintermann, J.; Spirig, C.; Jordan, A.; Kuhn, U.; Ammann, C.; Neftel, A. Eddy covariance flux measurements of ammonia by high temperature chemical ionisation mass spectrometry. *Atmos. Meas. Tech.* **2011**, *4*, 599−616.

(25) Whitehead, J. D.; Twigg, M.; Famulari, D.; Nemitz, E.; Sutton, M. A.; Gallagher, M. W.; Fowler, D. Evaluation of laser absorption spectroscopic techniques for eddy covariance flux measurements of ammonia. *Environ. Sci. Technol.* **2008**, *42*, 2041−2046.

(26) Ferrara, R.; Loubet, B.; Di Tommasi, P.; Bertolini, T.; Magliulo, V.; Cellier, P.; Eugster, W.; Rana, G. Eddy covariance measurement of ammonia fluxes: Comparison of high frequency correction methodologies. *Agric. For. Meteorol.* **2012**, *158*, 30−42.

(27) Ferrara, R. M.; Carozzi, M.; Di Tommasi, P.; Nelson, D. D.; Fratini, G.; Bertolini, T.; Magliulo, V.; Acutis, M.; Rana, G. Dynamics of ammonia volatilisation measured by eddy covariance during slurry spreading in north Italy. *Agric., Ecosyst. Environ.* **2016**, *219*, 1−13.

(28) Moravek, A.; Singh, S.; Pattey, E.; Pelletier, L.; Murphy, J. G. Measurements and quality control of ammonia eddy covariance fluxes: a new strategy for high-frequency attenuation correction. *Atmos. Meas. Tech.* **2019**, *12*, 6059−6078.

(29) von Bobrutzki, K.; Braban, C. F.; Famulari, D.; Jones, S. K.; Blackall, T.; Smith, T. E. L.; Blom, M.; Coe, H.; Gallagher, M.; Ghalaieny, M.; McGillen, M. R.; Percival, C. J.; Whitehead, J. D.; Ellis, R.; Murphy, J.; Mohacsi, A.; Pogany, A.; Junninen, H.; Rantanen, S.; Sutton, M. A.; Nemitz, E. Field inter-comparison of eleven atmospheric ammonia measurement techniques. *Atmos. Meas. Tech.* **2010**, *3*, 91−112.

(30) Sun, K.; Tao, L.; Miller, D. J.; Pan, D.; Golston, L. M.; Zondlo, M. A.; Griffin, R. J.; Wallace, H. W.; Leong, Y. J.; Yang, M. M. Vehicle emissions as an important urban ammonia source in the United States and China. *Environ. Sci. Technol.* **2017**, *51*, 2472−2481.

(31) Golston, L. M.; Pan, D.; Sun, K.; Tao, L.; Zondlo, M. A.; Eilerman, S. J.; Peischl, J.; Neuman, J. A.; Floerchinger, C. Variability of

https://doi.org/10.1021/acs.est.0c05749
Environ. Sci. Technol. 2021, 55, 7776−7785

ammonia and methane emissions from animal feeding operations in northeastern Colorado. *Environ. Sci. Technol.* **2020**, *54*, 11015−11024.
(32) Sun, K.; Tao, L.; Miller, D. J.; Zondlo, M. A.; Shonkwiler, K. B.; Nash, C.; Ham, J. M. Open-path eddy covariance measurements of ammonia fluxes from a beef cattle feedlot. *Agric. For. Meteorol.* **2015**, *213*, 193−202.
(33) Stratton, J. J.; Ham, J.; Borch, T. Ammonia Emissions from Subalpine Forest and Mountain Grassland Soils in Rocky Mountain National Park. *J. Environ. Qual.* **2018**, *47*, 778−785.
(34) Müller, M.; Mikoviny, T.; Feil, S.; Haidacher, S.; Hanel, G.; Hartungen, E.; Jordan, A.; Märk, L.; Mutschlechner, P.; Schottkowsky, R.; Sulzer, P.; Crawford, J. H.; Wisthaler, A. A compact PTR-ToF-MS instrument for airborne measurements of volatile organic compounds at high spatiotemporal resolution. *Atmos. Meas. Tech.* **2014**, *7*, 3763−3772.
(35) Mauder, M.; Cuntz, M.; Drüe, C.; Graf, A.; Rebmann, C.; Schmid, H. P.; Schmidt, M.; Steinbrecher, R. A strategy for quality and uncertainty assessment of long-term eddy-covariance measurements. *Agric. For. Meteorol.* **2013**, *169*, 122−135.
(36) Moore, C. J. Frequency response corrections for eddy correlation systems. *Boundary Layer Meteorol.* **1986**, *37*, 17−35.
(37) Liu, H.; Peters, G.; Foken, T. New equations for sonic temperature variance and buoyancy heat flux with an omnidirectional sonic anemometer. *Boundary Layer Meteorol.* **2001**, *100*, 459−468.
(38) Webb, E. K.; Pearman, G. I.; Leuning, R. Correction of flux measurements for density effects due to heat and water vapour transfer. *Q. J. R. Meteorol. Soc.* **1980**, *106*, 85−100.
(39) Burba, G.; Anderson, T.; Komissarov, A. Accounting for spectroscopic effects in laser-based open-path eddy covariance flux measurements. *Global Change Biol.* **2019**, *25*, 2189−2202.
(40) Kljun, N.; Calanca, P.; Rotach, M.; Schmid, H. A simple parameterisation for flux footprint predictions. *Boundary Layer Meteorol.* **2004**, *112*, 503−523.
(41) Langford, B.; Acton, J.; Ammann, C.; Valach, A.; Nemitz, E. Eddy-covariance data with low signal-to-noise ratio: time-lag determination, uncertainties and limit of detection. *Atmos. Meas. Tech.* **2015**, *8*, 4197−4213.
(42) Eilerman, S. J.; Peischl, J.; Neuman, J. A.; Ryerson, T. B.; Aikin, K. C.; Holloway, M. W.; Zondlo, M. A.; Golston, L. M.; Pan, D.; Floerchinger, C. Characterization of ammonia, methane, and nitrous oxide emissions from concentrated animal feeding operations in Northeastern Colorado. *Environ. Sci. Technol.* **2016**, *50*, 10885−10893.
(43) Wang, R.; Guo, X.; Pan, D.; Kelly, J. T.; Bash, J. O.; Sun, K.; Paulot, F.; Clarisse, L.; Van Damme, M.; Whitburn, S.; Coheur, P.-F.; Clerbaux, C.; Zondlo, M. A. Monthly patterns of ammonia over the contiguous United States at 2 km resolution. *Geophys. Res. Lett.* **2020**, *48*, No. e2020GL090579.
(44) Thompson, T. M.; Rodriguez, M. A.; Barna, M. G.; Gebhart, K. A.; Hand, J. L.; Day, D. E.; Malm, W. C.; Benedict, K. B.; Collett, J. L., Jr; Schichtel, B. A. Rocky Mountain National Park reduced nitrogen source apportionment. *J. Geophys. Res.: Atmos.* **2015**, *120*, 4370−4384.
(45) Environmental Modeling Center/National Centers for Environmental Prediction/National Weather Service/NOAA/US Department of Commerce. NCEP North American Mesoscale (NAM) 12 km Analysis. In *Research Data Archive at the National Center for Atmospheric Research*; Computational and Information Systems Laboratory: Boulder, CO, 2015.
(46) Bresenham, J. E. Algorithm for computer control of a digital plotter. *IBM Syst. J.* **1965**, *4*, 25−30.
(47) Gebhart, K. A.; Malm, W. C.; Rodriguez, M. A.; Barna, M. G.; Schichtel, B. A.; Benedict, K. B.; Collett, J. L.; Carrico, C. M. Meteorological and back trajectory modeling for the Rocky Mountain atmospheric nitrogen and sulfur study II. *Adv. Meteorol.* **2014**, *2014*, No. 414015.
(48) Massad, R.-S.; Nemitz, E.; Sutton, M. Review and parameterisation of bi-directional ammonia exchange between vegetation and the atmosphere. *Atmos. Chem. Phys.* **2010**, *10*, 10359−10386.
(49) Schrader, F.; Erisman, J. W.; Brümmer, C. Towards a coupled paradigm of NH3-CO2 biosphere-atmosphere exchange modelling. *Global Change Biol.* **2020**, *26*, 4654−4663.
(50) Pleim, J. E.; Ran, L.; Appel, W.; Shephard, M. W.; Cady-Pereira, K. New bidirectional ammonia flux model in an air quality model coupled with an agricultural model. *J. Adv. Model. Earth Syst.* **2019**, *11*, 2934−2957.
(51) Wentworth, G. R.; Murphy, J. G.; Benedict, K. B.; Bangs, E. J.; Collett, J. L., Jr The role of dew as a night-time reservoir and morning source for atmospheric ammonia. *Atmos. Chem. Phys.* **2016**, *16*, 7435−7449.
(52) Pleim, J. E.; Bash, J. O.; Walker, J. T.; Cooter, E. J. Development and evaluation of an ammonia bidirectional flux parameterization for air quality models. *J. Geophys. Res.: Atmos.* **2013**, *118*, 3794−3806.
(53) Moffat, A. M.; Papale, D.; Reichstein, M.; Hollinger, D. Y.; Richardson, A. D.; Barr, A. G.; Beckstein, C.; Braswell, B. H.; Churkina, G.; Desai, A. R. Comprehensive comparison of gap-filling techniques for eddy covariance net carbon fluxes. *Agric. For. Meteorol.* **2007**, *147*, 209−232.
(54) Flechard, C.; Spirig, C.; Neftel, A.; Ammann, C. The annual ammonia budget of fertilised cut grassland—Part 2: Seasonal variations and compensation point modeling. *Biogeosciences* **2010**, *7*, 537−556.
(55) Toth, J. J.; Johnson, R. H. Summer surface flow characteristics over northeast Colorado. *Mon. Weather Rev.* **1985**, *113*, 1458−1469.
(56) Ammann, C.; Brunner, A.; Spirig, C.; Neftel, A. Water vapour concentration and flux measurements with PTR-MS. *Atmos. Chem. Phys.* **2006**, *6*, 4643−4651.
(57) Benedict, K. B.; Prenni, A. J.; Carrico, C. M.; Sullivan, A. P.; Schichtel, B. A.; Collett, J. L., Jr Enhanced concentrations of reactive nitrogen species in wildfire smoke. *Atmos. Environ.* **2017**, *148*, 8−15.
(58) Seabold, S.; Perktold, J. In *Statsmodels: Econometric and Statistical Modeling with Python*, Proceedings of the 9th Python in Science Conference; Austin, TX, 2010; p 61.

https://doi.org/10.1021/acs.est.0c05749
Environ. Sci. Technol. 2021, 55, 7776−7785